ZrO$_2$ Is Preferred over TiO$_2$ as Support for the Ru-Catalyzed Hydrogenation of Levulinic Acid to γ-Valerolactone

Jamal Ftouni,[†] Ara Muñoz-Murillo,[†] Andrey Goryachev,[‡] Jan P. Hofmann,[‡] Emiel J. M. Hensen,[‡] Li Lu,[§] Christopher J. Kiely,[§] Pieter C. A. Bruijnincx,*,[†] and Bert M. Weckhuysen*,[†]
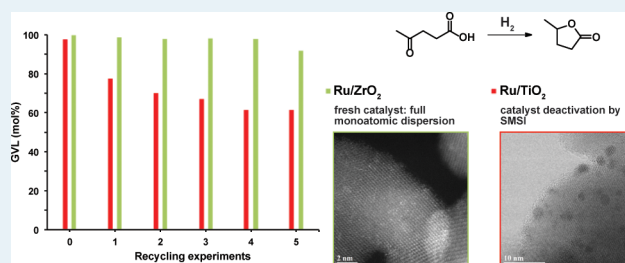
[†]Inorganic Chemistry and Catalysis, Debye Institute for Nanomaterials Science, Utrecht University, Universiteitsweg 99, 3584 CG Utrecht, The Netherlands

[‡]Laboratory of Inorganic Materials Chemistry, Department of Chemical Engineering and Chemistry, Eindhoven University of Technology, Postbox 513, 5600 MB Eindhoven, The Netherlands

[§]Department of Materials Science and Engineering, Lehigh University, 5 East Packer Avenue, Bethlehem, Pennsylvania 18015, United States

ABSTRACT: Catalyst stability in the liquid phase under polar conditions, typically required for the catalytic conversion of renewable platform molecules, is a major concern but has been only sparsely studied. Here, the activity, selectivity, and stability of Ru-based catalysts supported on TiO$_2$, ZrO$_2$, and C in the conversion of levulinic acid (LA) to γ-valerolactone (GVL) has been studied at 30 bar of H$_2$ and 423 K in dioxane as solvent. All catalysts showed excellent yields of GVL when used fresh, but only the Ru/ZrO$_2$ catalyst could maintain these high yields upon multiple recycling. Surprisingly, the widely used Ru/TiO$_2$ catalyst showed quick signs of deactivation already after the first catalytic test. XPS, CO/FT-IR, TGA, AC-STEM, and physisorption data showed that the partial deactivation is not due to Ru sintering or coking but rather due to reduction of the titania support in combination with partial coverage of the Ru nanoparticles, i.e. due to a detrimental strong metal−support interaction. In contrast, the zirconia support showed no signs of reduction and displayed high morphological and structural stability even after five recycling tests. Remarkably, in the fresh Ru/ZrO$_2$ catalyst, Ru was found to be fully atomically dispersed on the fresh catalyst even at 1 wt % Ru loading, with some genesis of Ru nanoparticles being observed upon recycling. Further studies with the Ru/ZrO$_2$ catalyst showed that dioxane can be readily replaced by more benign solvents, including GVL itself. The addition of water to the reaction mixture was furthermore shown to promote the selective hydrogenation reaction.

KEYWORDS: levulinic acid, catalyst stability, strong metal−support interaction, biomass, single-atom catalysis

1. INTRODUCTION

Many research efforts are currently being devoted to the development of efficient catalytic conversion routes for the production of renewable fuels and chemicals from lignocellulosic biomass. In this respect, the platform molecule γ-valerolactone (GVL) has attracted much attention, as it can be used in the chemical industry either directly or, after further upgrading, as a fuel additive, food ingredient, nylon intermediate, or renewable solvent.[1,2] GVL can be obtained by gas- or liquid-phase hydrogenation of levulinic acid (LA) using a suitable metal-based catalyst and a hydrogen source. Most of the literature examples describing liquid-phase LA hydrogenation to GVL make use of molecular hydrogen or liquid hydrogen donors such as formic acid[3−5] or alcohols such as ethanol, butanol, and isopropyl alcohol.[6−8] Such liquid-phase LA hydrogenations are typically run in the presence of either organic or aqueous solvent, but reactions in neat LA have also been reported.[9,10] In the past few years, many different active phases, including both noble and non-noble metals, were tested for the reduction of LA to GVL;[11−16] ruthenium-based catalysts

have nonetheless emerged as the catalysts of choice, as they are typically the most active and selective.[10,17−19] For example, Manzer compared the activity of carbon supported on Ir, Rh, Pd, Ru, Pt, Re, and Ni catalysts and found Ru/C to perform the best.[17] The commercial availability of the latter has further contributed to its extensive use in the literature.[10,17,18]

While most of these studies are concerned mainly with activity/selectivity, the third critical parameter of catalyst performance, i.e. stability, has been much less investigated.[20] For Ru/C, the limited number of examples available already shows, however, that stability is an issue and depends strongly on the choice of experimental conditions employed, with the type of solvent used being particularly important. Indeed, Ru/C reuse experiments in ethanol showed a drop in both the selectivity to GVL as well as the LA conversion rate.[10] A similar result was obtained using methanol as a solvent, in which Ru/C

also showed quick deactivation already upon the first recycling.[18] The same was seen by Wettstein et al. using 2-sec-butylphenol as the solvent, with deactivation of the Ru/C catalyst in this case being irreversible, as reactivation under H_2 flow and high temperature did not restore its activity.[21] Likewise, also in water, deactivation of Ru/C was observed.[22] On the other hand, Upare et al. showed that Ru/C maintained its activity in dioxane under continuous-flow, vapor-phase conditions for 10 days on stream, with these stability tests being performed at full LA conversion, however.[23] More generally, it should be noted though that carbon supports would not survive the multiple regeneration cycles required for catalyst reactivation by burning off coke at high temperatures, which makes them after all less suitable for industrial use.[24]

In general, catalyst performance in LA hydrogenation is greatly influenced by the choice of support, a topic that has recently attracted some attention, but again with more emphasis on activity and selectivity than on stability. As an example of the latter, Lange et al., for example, showed that SiO_2, TiO_2 and ZrO_2 supports retained their structural integrity after exposure to hot levulinic acid, while others, including alumina and silica–alumina, did not. Of these, TiO_2 has attracted the most attention and has emerged as an attractive alternative to carbon as support.[24] We previously showed, for example, that Ru/TiO_2 (P25) gave excellent GVL yields both in dioxane as solvent and under more severe conditions including reactions run in neat LA and the LA mimic 2-ethylhexanoic acid.[9] Analysis of the spent Ru/TiO_2 catalyst showed the metal phase to be rather stable with very limited sintering and no significant leaching being observed even under the most severe conditions.[9] Catalyst reuse was not yet included in these studies. In the work of Al-Shaal et al. Ru catalysts supported on both pure rutile titania (with a low specific surface area) and P25-titania were compared under the same experimental conditions (i.e., T = 298 K) in ethanol or in water/ethanol. No conversion was seen with the pure rutile support, while good LA conversion and excellent GVL selectivity were obtained with TiO_2 (P25).[10] More facile substrate adsorption on TiO_2 (P25) or a high Ru dispersion was held responsible for this effect. A more detailed study of the influence of the titania phase was reported by Ruppert et al., who ran the hydrogenation reaction at low temperature (303–343 K) in water. The highest GVL yields were obtained with a 90/10 anatase/rutile titania mixture and with pure rutile, while pure anatase-based catalysts performed much less well. The obtained results were linked to both the electronic properties of the support and the dispersion of Ru particles on the oxide surface.[25] Again, the focus in this study was on initial activity and no stability tests were performed.

The deactivation of metal-based supported catalysts is influenced by many different factors, including the type and the size of the metallic particles and their interaction with the support.[26] Stabilization strategies studied for Ru-based catalysts have included improving the metal phase stability by adding another metal to prevent irreversible deactivation by sintering.[27,28] Wettstein et al., for example, showed that addition of Sn to Ru/C led to much improved stability, albeit with reduced activity.[21] The same strategy was adopted by Yang et al., who reported on a highly stable Ru–Ni bimetallic catalyst supported on ordered mesoporous carbon which could be recycled up to 15 times in batch reactions using water as solvent.[29] Braden et al. in turn showed a Ru-Re/C catalyst to display improved stability even in the presence of some traces of sulfuric acid, a

small amount of which rapidly deactivated the Ru/C monometallic catalyst.[30] Recently, we showed that a Ru-Pd nanoalloy supported on titania proved highly active, selective, and stable upon recycling.[27] Yao et al. investigated sulfonated poly(ether sulfone) (SPES), which showed superior performance over Ru/C in the hydrogenation of LA to GVL in water, while no deactivation was seen for Ru/SPES after five recycling tests.[31] Deng et al. prepared a Ru-based catalyst supported on a carbon or silica surface grafted with (mercaptopropyl)-trimethoxysilane or (3-aminopropyl)trimethoxysilane, moieties which served as anchoring agents for the supported Ru nanoparticles. The latter catalyst materials showed improved performance and high stability in the aqueous hydrogenation of LA during multiple recycling tests.[3] More extensive, structural studies on support-dependent mechanisms of deactivation are very limited, however. Abdelrahman et al., in one such example, recently reported on such a detailed study using Ru supported on carbon, silica, alumina, and titania, distinguishing irreversible, sintering-related deactivation as well as reversible deactivation, both of which were support dependent.[26]

In the present study, we report on the effect of the choice of support on the stability of monometallic Ru catalysts. The performance and stability of Ru/TiO_2 (P25) was compared to a benchmark, commercial Ru/C catalyst in the selective reduction of LA into GVL, using dioxane as a solvent. Rather surprisingly, Ru/TiO_2 showed considerable deactivation upon reuse, which could be attributed to reduction of the support and partial coverage of the metal nanoparticles. Ru/ZrO_2, a support which was previously shown to withstand severe liquid-phase conditions well,[24,32] is shown to be an excellent alternative for this reaction.

2. EXPERIMENTAL SECTION

2.1. Materials. All chemicals were used as received without any further purification. For the catalytic testing the following chemicals have been used: levulinic acid (98%), 1,4-dioxane (99+%, containing 0.05% of H_2O), and anhydrous 1,4-dioxane (<99.8%) from Alfa Aesar. Anhydrous THF (unstabilized) was obtained from an MBRAUN solvent purification system. γ-Valerolactone (99%), γ-hexalactone (<98%), γ-octalactone (<97%), and δ-hexalactone (<98%) were obtained from Sigma-Aldrich. Anisole (99%), used as an internal standard, was purchased from Acros Organics. For the preparation of the catalyst materials the following chemicals have been used: ruthenium(III) nitrosyl nitrate ($RuNO(NO_3)_3$/Ru 31.3%) was obtained from Alfa Aesar, while the supports TiO_2 (P25) and ZrO_2 (monoclinic) Daiichi Kikenso RC-100 were obtained from Degussa. The commercial Ru/C (with an average Ru diameter of 2.5 nm)[33] was obtained from Aldrich and used as received. Technical grade acetone (>99%), used for washing the catalyst, was purchased from Interchema.

2.2. Catalyst Preparation. Two 1 wt % Ru catalysts supported on TiO_2 (P25) and monoclinic ZrO_2 were prepared using a wet impregnation procedure. First, the supports were crushed and then dried for 2 h at 393 K, after which the support was dispersed in distilled water with stirring (450 rpm) for 30 min. 10 mL of the precursor solution was added to the suspended support dropwise, after which the mixture was allowed to stand for 1 h. After elimination of the water under vacuum at 333 K, the catalyst was dried at 333 K overnight and calcined at 773 K for 3.5 h with a heating ramp of 5 K/min under an N_2 flow of 100 mL/min, followed by its reduction at 723 K for 5 h under an H_2 flow of 80 mL/min.

2.3. Catalyst Characterization. Thermal gravimetric analysis (TGA) was performed with a Perkin-Elmer Pyris 1 apparatus. The sample was initially heated to 423 K for 1 h with a temperature ramp of 10 K/min under a 20 mL/min flow of Ar to exclude physisorbed water and acetone, followed by a ramp of 5 K/min to 873 K under a 10 mL/min flow of O_2 to burn off any organic deposits formed. N_2 physisorption isotherms were recorded to determine surface areas and pore volumes with a Micromeritics Tristar 3000 setup operating at 77 K. The samples were outgassed prior to performing the measurements for 20 h at 573 K under an N_2 flow. Surface areas were determined using the Brunauer−Emmett−Teller (BET) theory, while pore volumes (cm^3/g) were determined by the BJH method. Samples for examination by scanning transmission electron microscopy (STEM) were prepared by dry dispersing the catalyst powder onto holey carbon supported by a 300 mesh copper TEM grid. Bright field (BF) and high angle annular dark field (HAADF) STEM images were taken using an aberration-corrected JEM ARM 200CF microscope operating at 200 kV. Particle size distribution analysis was performed from the electron micrographs using ImageJ. Scanning electron microscopy (SEM) images were taken on a FEI Quanta 3D FEG microscope at an accelerating voltage of 5 kV without additional coating of the surface. The X-ray photoelectron spectroscopy (XPS) measurements were carried out on a Thermo Scientific K-Alpha spectrometer, equipped with a monochromatic small-spot X-ray source and a 180° double-focusing hemispherical analyzer with a 128-channel detector. Spectra were obtained using an aluminum anode (Al $K\alpha$ = 1486.6 eV) operating at 72 W and a spot size of 400 μm; samples were not handled under an inert atmosphere and should be considered passivated. Survey scans were measured at constant pass energy of 200 eV and region scans at 50 eV. The background pressure of the UHV chamber was 2×10^{-8} mbar. As the C 1s and Ru 3d core level regions overlap, the Ru/TiO_2 spectra were calibrated using the well-isolated Ru $3d_{5/2}$ peak at 280.0 eV. ZrO_2-supported catalysts were calibrated by setting the C 1s adventitious carbon position to 284.8 eV. Component peak areas have been normalized on the basis of atomic sensitivity factors: C 1s, 0.25; O 1s, 0.66; Ru 3d, 3.6; Ru 3p, 1.3; Ti 2p, 1.8; Zr 3d, 2.1.[34] Powder X-ray diffraction (XRD) patterns were measured with a Bruker D8 Advance powder X-ray diffractometer equipped with automatic divergence slits, a Vantec detector, and a cobalt $K\alpha_{1,2}$ (λ = 1.78897/1.79026 Å) source. Diffraction patterns were collected between 5 and 40° or between 5 and 55° 2θ with an increment of 0.017 (in 2θ) and an acquisition time of 1 s per step. Fourier transform infrared (FT-IR) spectra in transmission mode were recorded on a PerkinElmer 2000 instrument. Samples were pressed under 3.5 tons for 15 s to achieve self-supporting wafers (12−28 mg/13 mm diameter). The wafer was positioned in a well-sealed cell with CaF_2 windows and posteriorly activated at 873 K (5 K/min) under high vacuum (10^{-6} bar). Subsequently, the cell was cooled to 85 K. Spectra were taken upon CO (10% in He, purity 99.9%) adsorption on the sample, at increasing pressures.[22]

2.4. Catalyst Testing. All reactions were run in a 50 mL Parr batch autoclave at a temperature of 423 K for 3 h using a H_2 pressure of 30 bar and a stirring speed of 1250 rpm. It was previously shown that in this setup LA conversion is essentially independent of the stirrer speed above 900 rpm.[9] In a typical reaction, the batch autoclave reactor was loaded with the catalyst, substrate, and solvent using a substrate (LA) to catalyst

(bulk Ru) ratio of 1000. Then, the autoclave was purged three times with Ar, after which the reaction mixture was heated to the reaction temperature and charged with H_2. This was taken as the starting point of the reaction; during the reaction samples were taken regularly and filtered and 1 wt % of anisole was added as internal standard. At the end of the reaction, the autoclave was cooled rapidly to room temperature in an ice bath, after which the remaining H_2 was released. The catalyst was separated by filtration (filters of 0.45 μm), washed with acetone, and dried overnight at 333 K in air. The reaction products were analyzed using a Shimadzu GC-2010A gas chromatograph equipped with a CPWAX 57-CB column (25 m × 0.2 mm × 0.2 μm) and FID detector, using authentic samples for calibration. The majority of the tests were performed using 1,4-dioxane (27 g) as a solvent and 10 wt % of levulinic acid (3 g, 25.8 mmol) over a series of 1 wt % of Ru supported catalysts. For all three catalysts ($Ru_{5\%}/C$, $Ru_{1\%}/TiO_2$, and $Ru_{1\%}/ZrO_2$), the amount of catalyst added to the reaction medium was such that a molar LA to Ru (bulk) ratio of 1000 was obtained. TOF values were calculated from the initial rate (measured after 0.5 h) and metal dispersion, as estimated from the (S)TEM data.[27] Additional tests were performed using other organic solvents (i.e., tetrahydrofuran, γ-hexalactone, δ-hexalactone, and δ-valerolactone) under otherwise similar experimental conditions. For the experiment performed with GVL as a solvent, the GVL yield was calculated on the basis of the LA conversion and the absence of any byproducts.

3. RESULTS AND DISCUSSION

3.1. Effect of the Support on Catalyst Performance. Levulinic acid hydrogenation reactions were conducted under batch conditions in dioxane. Given the many different reaction conditions reported for the LA to GVL reaction,[1] we first varied the reaction temperature and H_2 pressure with the commercial, benchmark Ru/C to find suitable standard conditions for the study of the influence of support on performance. As expected and shown before, the catalytic efficiency was found to be highly sensitive to reaction temperature but did not much depend on H_2 pressure.[22]

At 373 K, full LA conversion was only reached after 24 h, while at 323 K less than 20% GVL was obtained after the same time interval. Instead, full conversion and quantitative GVL yields were reached after a convenient 3 h of reaction at 423 K. The results shown in Figure 1a depict the influence of reaction temperature at a fixed H_2 pressure of 30 bar. Variation of the H_2 pressure from 20 to 40 bar at 423 K had a modest effect, all giving nearly full GVL yields after 3 h. This is in line with the findings of Yan et al., who noted no difference in GVL yields above 12 bar of H_2 in reactions run in water.[18] Standard reaction conditions were thus set at 423 K, P_{H_2} = 30 bar, and a fixed molar LA/bulk Ru ratio of 1000. Under these experimental conditions, the performance of the benchmark Ru/C catalyst was compared to that of Ru/TiO_2 and Ru/ZrO_2 solids, both synthesized by a standard wet-impregnation method. Characterization data for these last two catalysts can be found in Table 1.

The production of GVL as a function of time is shown in Figure 1b for the three catalysts. All three catalysts did show near-quantitative GVL yields after 3 h, with TOFs varying in the order Ru/C (0.53 s^{-1}) > Ru/TiO_2 (0.29 s^{-1}) > Ru/ZrO_2 (0.24 s^{-1}). Notably, already after the first use, the recovered Ru/TiO_2 catalyst was found to have changed color from gray to
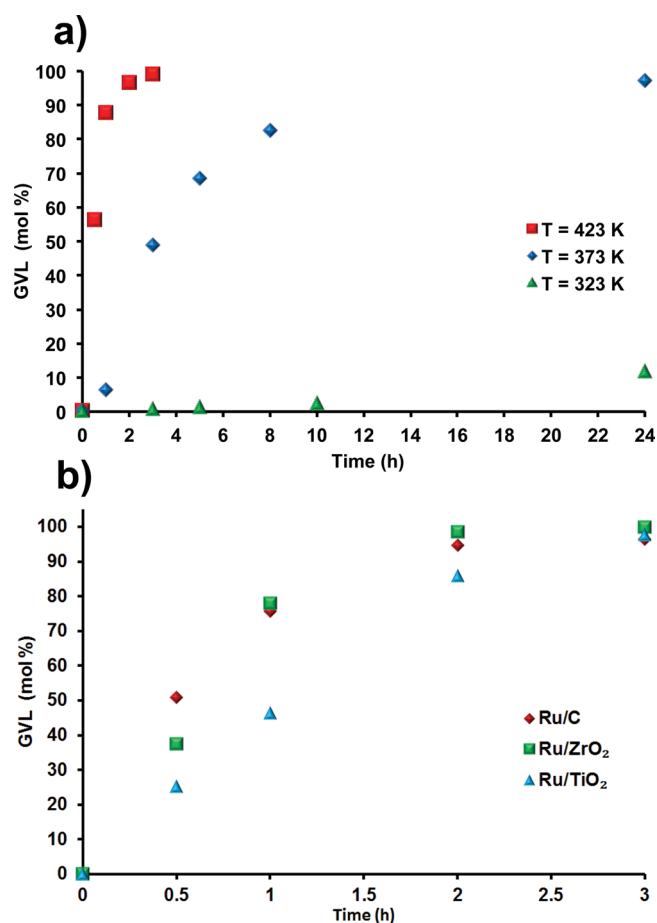
Figure 1. GVL yields (a) as a function of time and temperature using commercial Ru/C and (b) as a function of time using Ru-based catalysts supported on ZrO$_2$, TiO$_2$, and C. Experimental conditions: 10 wt % LA; LA/Ru = 1000; T = 423 K, and P_{H_2} = 30 bar.

Figure 2. GVL yields as a function of reuse for the Ru-based catalysts supported on ZrO$_2$, TiO$_2$, and C. Experimental conditions: 10 wt % LA; LA/Ru = 1000; T = 423 K; P_{H_2} = 30 bar, and t = 3 h. The tests performed at lower conversion with Ru/C and Ru/ZrO$_2$ were run at 373 K for 3 h.

dark black. In contrast, the gray Ru/ZrO$_2$ solid remained visually unchanged after the reaction. This change in color of the Ru/TiO$_2$ material already pointed at its instability, which was further evidenced upon its recycling. The origin of the darkening is described in detail below (see section 4).

The stability of the Ru/TiO$_2$, Ru/C, and Ru/ZrO$_2$ catalysts under the applied batch conditions was assessed by multiple catalyst recycling tests. The solid was recovered after the reaction, simply washed with acetone, dried at 333 K overnight, and used again. Under these conditions, Ru/C showed only a small drop in GVL yield from 96 to 92% upon the fifth reuse (Figure 2). Stability tests at lower conversion (3 h at 373 K) nonetheless showed a clear deactivation of the Ru/C catalyst, with GVL yields dropping from nearly 50% to 20% in the fifth recycling test, still with full GVL selectivity. TEM measure-
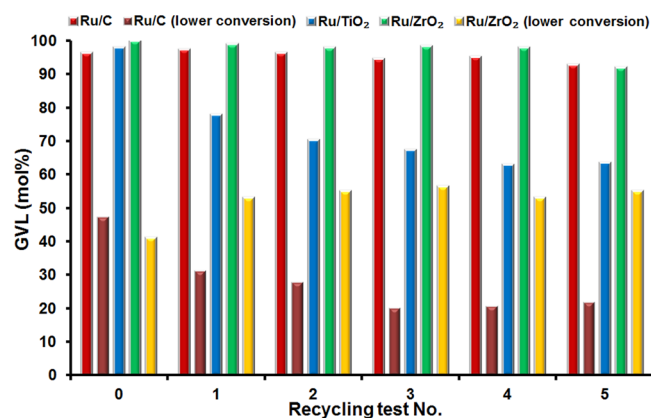
ments performed on both the fresh Ru/C and the Ru/C recycled five times (at lower conversion) excluded sintering as the cause of deactivation, as no difference was seen in particle size between the two samples, with averages of 1.7 ± 0.4 and 1.7 ± 0.7 nm, respectively. Physisorption measurements showed some changes in the support, with the surface area dropping from 777 to 674 m^2/g after recycling five times and t-plot micropore volume dropping from 0.22 to 0.18 cm^3/g.

In sharp contrast, even at high conversion, three runs were already sufficient to show that the Ru/TiO$_2$ catalyst was considerably less stable, showing a drop of ∼30% in GVL yield. After the fifth recycling, a GVL yield of only 63% was obtained. Ru/ZrO$_2$, on the other hand, proved to be highly stable and near-quantitative GVL yields were obtained up to the fourth recycling run. The fifth recycling test showed a slight drop, similar to the slight (but more gradual) deactivation noticed for Ru/C at high conversion. This drop in activity could be attributed to the buildup of carbonaceous deposits as shown in Table 1. For Ru/ZrO$_2$, recycling tests were also performed at lower conversion, again showing stable performance, with the yield actually going up slightly upon the first recycling. A single regeneration attempt by reduction at 723 K of both the Ru/TiO$_2$ and Ru/ZrO$_2$ catalysts recycled five times proved inconclusive. Some but not full restoration of the activity was seen for Ru/TiO$_2$ (78% GVL after regeneration), while regenerated Ru/ZrO$_2$ showed the same yield as that after five recycle runs.

3.2. Effect of the Solvent. LA hydrogenation reactions are sometimes run neat but are more often carried out on dilution in either water or an organic solvent. The choice of solvent is very important both from an environmental point of view, e.g.

Table 1. Physicochemical Properties of the Fresh and Spent Ru/TiO$_2$ (Recycled Three Times) and Ru/ZrO$_2$ (Recycled Five Times) Catalysts under Study

sample	BET (m^2/g)	total pore volume^a (cm^3/g)	av pore diameter^a(nm)	Ru diameter^b (nm)	wt loss^c (%)
Ru/TiO$_2$ (fresh)^f	79	0.22	9.9	2.7 ± 1.1	
Ru/TiO$_2$ (spent)^f	45	0.36	28.8	2.1 ± 0.7	3
Ru/ZrO$_2$ (fresh)^f	94	0.24	9.2	d	
Ru/ZrO$_2$ (spent)^f	87	0.22	9.2	2.8 ± 0.9^e	7

^{a}Data obtained by the BJH method. ^{b}Images obtained using STEM. ^{c}Data determined by TGA. ^{d}Fully monoatomically dispersed. ^{e}Atomic Ru not included in the average particle size. ^{f}Samples dried at 573 K prior to analysis.

the solvent typically dominates the footprint of a process, and from an upscaling point of view, as the use of some solvents on an industrial scale may be complicated (e.g., by their toxicity).[35] Dioxane, for example, is a very convenient solvent for small-scale catalyst development studies, but its toxicity makes it less suited for larger-scale utilization.

We thus investigated alternatives to dioxane including THF and different bio-based γ- and δ-lactones (Figure 3), including
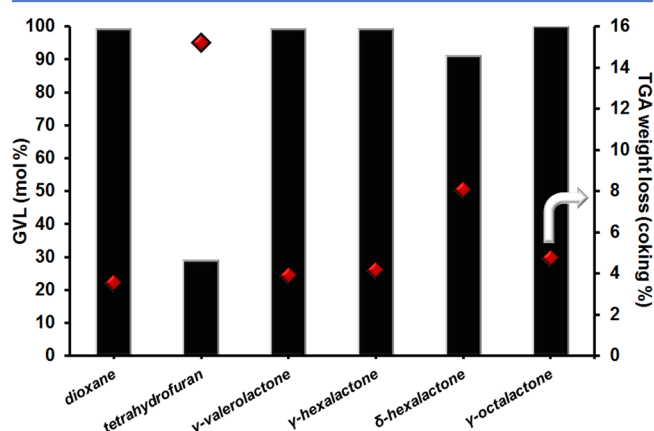

Figure 3. GVL yields (bars) and TGA weight loss (%) (diamonds) as a function of solvent with Ru/ZrO$_2$. Experimental conditions: 10 wt % LA; LA/Ru = 1000; T = 423 K; P_{H_2} = 30 bar, and t = 3 h.

GVL itself under the same standard conditions.[36] GVL is being increasingly used as a green solvent in various catalytic conversions, having a high stability in the presence of water or oxygen and a low toxicity and flammability risk.[2]

The obtained results, presented in Figure 3, show that high GVL yields are obtained with all γ-lactones, including GVL; however, tetrahydrofuran and δ-hexalactone proved less suited and gave lower GVL yields, albeit still with full selectivity. The reduced performance of the last two solvents correlated well with the amount of carbonaceous deposits formed, as assessed by TGA analysis (Figure 3), with 8 and 15% weight loss detected for δ-hexalactone and THF, respectively. The spent catalysts from the runs in dioxane, γ-valerolactone, γ-hexalactone, and γ-octalactone showed much less carbon deposition (≤5%). TOF values were determined for GVL (0.10 s^{-1}), dioxane (0.24 s^{-1}), and γ-octalactone (0.26 s^{-1}), showing some small differences in activity for the selected solvents. The deactivation noted for THF most probably results from THF polymerization into a polyether polyol,[37] while the differences seen for the γ- and δ-lactones can be related to the ease of ring opening to the corresponding enoic acids, which might be more prone to coking.

The effect of added water on the performance of the Ru/ZrO$_2$ catalyst was also investigated, as water can be expected to be carried over from prior biomass pretreatment steps and is likely to influence catalyst performance. Different amounts of added water were tested, and anhydrous dioxane was included for comparison (Figure 4).

The results obtained after 1 h of reaction time clearly show water to have a positive effect on the catalysis, with the addition of 1 wt % already showing an increase in GVL yield of 25%. Yields further increase with the addition of 10 wt % water, resulting in near full conversion already after 1 h. Larger amounts of added water then led to a small drop in activity, as exemplified by the 50 wt % example. Note that in all cases
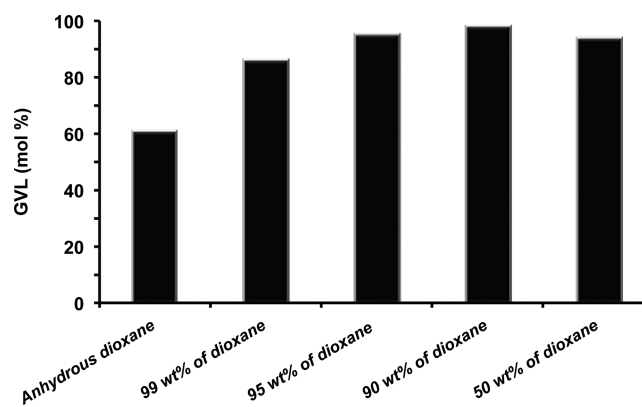

Figure 4. GVL yields as a function of the amount of water added to dioxane (total volume is kept constant) using Ru/ZrO$_2$. Experimental conditions: 10 wt % LA; LA/Ru = 1000; T = 423 K; P_{H_2} = 30 bar, and t = 1 h.

(near) quantitative GVL yields were obtained after 3 h, though. The obtained results are similar to those described recently by Tan et al., who also noted that water promoted the rate of LA hydrogenation and showed it to participate in the reaction.[38]

Michel et al. investigated the role of water in LA hydrogenation in a combined experimental and DFT study. These studies showed that the capability of Ru to hydrogenate acetone (taken as a model for LA) was strongly enhanced by the presence of a single chemisorbed water molecule.[39]

4. CATALYST CHARACTERIZATION: INSIGHT INTO STABILITY AND DEACTIVATION

To get more insight into the large differences in catalyst performance, the fresh and spent Ru/TiO$_2$ (recycled three times) and Ru/ZrO$_2$ (recycled five times) catalysts were characterized by N$_2$ physisorption, SEM, XPS, FT-IR after CO adsorption, and STEM. The N$_2$ physisorption measurements already showed a dramatic difference (Table 1). Indeed, the specific surface area of the Ru/TiO$_2$ catalyst recycled three times decreased remarkably in comparison to the fresh catalyst, while the pore diameter increased considerably. Importantly, the average diameter of the Ru nanoparticles in Ru/TiO$_2$ did not change much from the fresh sample (2.7 ± 1.1 nm) to the sample recycled three times (2.1 ± 0.7 nm), as measured by STEM. TGA analysis of the Ru/TiO$_2$ catalyst recycled three times furthermore showed 3% weight loss, suggesting that carbon deposition is limited. Taken together, these results suggest that the partial deactivation of the Ru/TiO$_2$ catalyst is not caused by loss of metallic surface area by sintering of Ru particles, nor is it likely the result of deposition of carbonaceous deposits. Instead, the partial deactivation of the catalyst is linked to a modification of the TiO$_2$ (P25) support.

In stark contrast, the changes in BET surface area and pore volume were found to be very minor for the Ru/ZrO$_2$ catalyst, showing only a slight decrease even after five recycling tests. TGA analysis showed 7% weight loss after six runs (five recycling tests), and these carbonaceous deposits might be the cause of the slight deactivation seen in Figure 2. SEM images of the Ru/ZrO$_2$ catalyst (data not shown) further highlight the structural integrity of this catalyst, with the same homogeneous size distribution of a few micrometers (1−3 μm) being observed for both the fresh and spent catalyst.

4.1. XPS Measurements. Further insights into the (lack of) change in catalyst structure were obtained from XPS

measurements on the fresh and recycled ruthenium catalysts supported on TiO_2 (recycled three times) and ZrO_2 (recycled five times). The fresh TiO_2-supported Ru catalyst contains mostly TiO_2 with Ti^{4+} species at the surface (Figure 5a), as indicated by the intense Ti $2p_{3/2}$ component at 459.0 eV. In addition to the dominant signal of Ti^{4+}, a small (12%) contribution of Ti^{3+} (Ti $2p_{3/2}$ component at 457.6 eV) can also be seen. The peak at 461.0 eV is the Ru $3p_{3/2}$ signal, which overlaps with the Ti 2p region.[40] The Ti 2p core level spectra of

the fresh and spent catalyst are very different. The change in color of the used Ru/TiO_2 catalyst that was noted above already pointed at the possibility of (partial) reduction of titania and formation of Ti^{3+} species.[41] The XP spectrum of the used catalyst indeed showed a large increase in the amount of Ti^{3+} after the reaction, as is evident from the Ti $2p_{3/2}$ peak at 458.0 eV.[42] The reducing conditions during LA hydrogenation thus apparently led to the reduction of a significant amount of Ti^{4+} to Ti^{3+}. Titania reduction has been reported to be facilitated by Ru by hydrogen spillover.[36,43−45] The Ti^{3+}/Ti^{4+} ratio increased by a factor of 10 from the fresh catalyst (0.14) to the spent catalyst (1.3), corresponding with a close to 5-fold increase in Ti^{3+} from 12 to 55%.

The signal of the Ru 3d core levels overlaps with the C 1s core levels (Figure 5b); C 1s spectra of adventitious carbon (AC) species were fitted according to the reported binding energies.[46] This overlap complicated both the analysis of the Ru 3d species as well as the charge correction, for which the C 1s peak of adventitious carbon (sp_3-CH, C−C) at 284.8 eV is usually used. The fresh Ru/TiO_2 sample contains mostly cationic Ru species (81% of total Ru 3d) as Ru^{4+} and $Ru^{\delta+}$ with $3d_{5/2}$ binding energies of 283.6 and 281.3 eV, respectively, as well as metallic Ru^0 with a $3d_{5/2}$ binding energy of 280.0 eV.[43,47] Note that as the samples were not rigorously kept under an inert atmosphere prior to XPS analysis, some changes in Ru oxidation state might have been induced by catalyst retrieval, handling, and transport. The relevance of the Ru oxidation state quantification is therefore limited and differences between samples should be treated with caution. The O 1s spectral region reveals three major contributions (Figure 5c), which can relate to organic/hydroxyl O (531.9−532.0 eV), Ti^{4+}-O (530.2−530.5 eV), and Ti^{3+}-O (529.0−529.3 eV) species. Oxygen from RuO_2 has a binding energy of 529.4 eV and would overlap with the Ti^{4+}-O component, and this cannot be resolved in light of the low Ru loading. The O 1s feature of fresh catalyst mainly consists of Ti^{4+}-O (70%) with a small amount of Ti^{3+}-O (10%). In line with the results above, after reduction the O 1s signal shows that part of the TiO_2 has been converted to Ti^{3+}-O, giving again the same Ti^{4+}/Ti^{3+} ratio as obtained from the Ti_{2p} region.

In contrast to the reduction of the support observed in the case of Ru/TiO_2, the ZrO_2 support of the Ru/ZrO_2 remained virtually unchanged upon use in the LA hydrogenation reaction (Figure 6a). The Zr 3d core level spectrum (Zr $3d_{5/2}$ at 181.8 eV) does not show a significant intensity change or new spectral features indicative of reduction following the LA hydrogenation reaction (Figure 6a). In keeping with this, the O 1s region for Ru/ZrO_2 was also not affected by the catalytic reaction, showing no significant change in either peak composition or intensities (Figure 6c). The major component O(I) corresponds to ZrO_2 (529.7−529.9 eV) and components O(II) (531.4−531.6 eV) and O(III) (532.8−533.3 eV) relate to organic or hydroxylic O and adsorbed water, respectively.[48]

The darkening of the Ru/TiO_2 catalyst can thus be attributed to a reduction of the support. Indeed, a reduction method has previously been developed by Chen et al. with the specific purpose of obtaining "black hydrogenated titanium oxide" for use in photocatalysis.[49] The reduction treatment in this particular case aims to enhance solar absorption by introducing disorder at the TiO_2 surface. This solid could be obtained via lengthy hydrogenation of TiO_2 under an H_2 atmosphere at elevated temperature (P_{H_2} = 20 bar, T = 673 K; t ≈ 120 h).
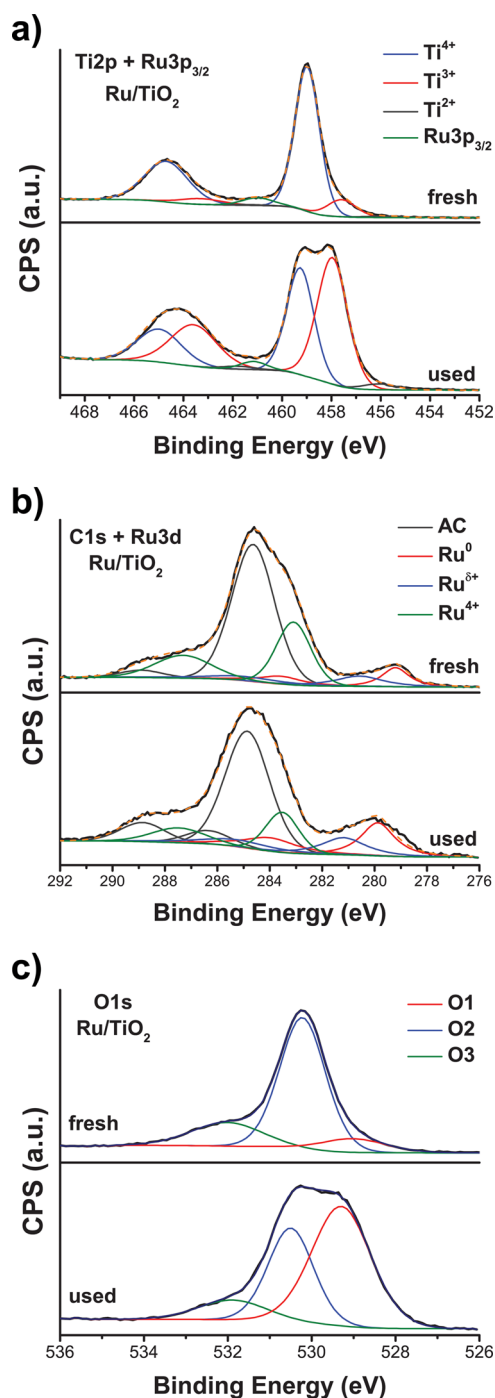
Figure 5. (a) Ti 2p and Ru $3p_{3/2}$ XP spectra, (b) C 1s and Ru 3d XP spectra, and (c) O 1s XP spectra (O1 refers to organic and hydroxylic O, O2 to stoichiometric TiO_2, and O3 to O in reduced $TiO_{2−x}$) of the fresh and three-times recycled Ru/TiO_2 catalysts.
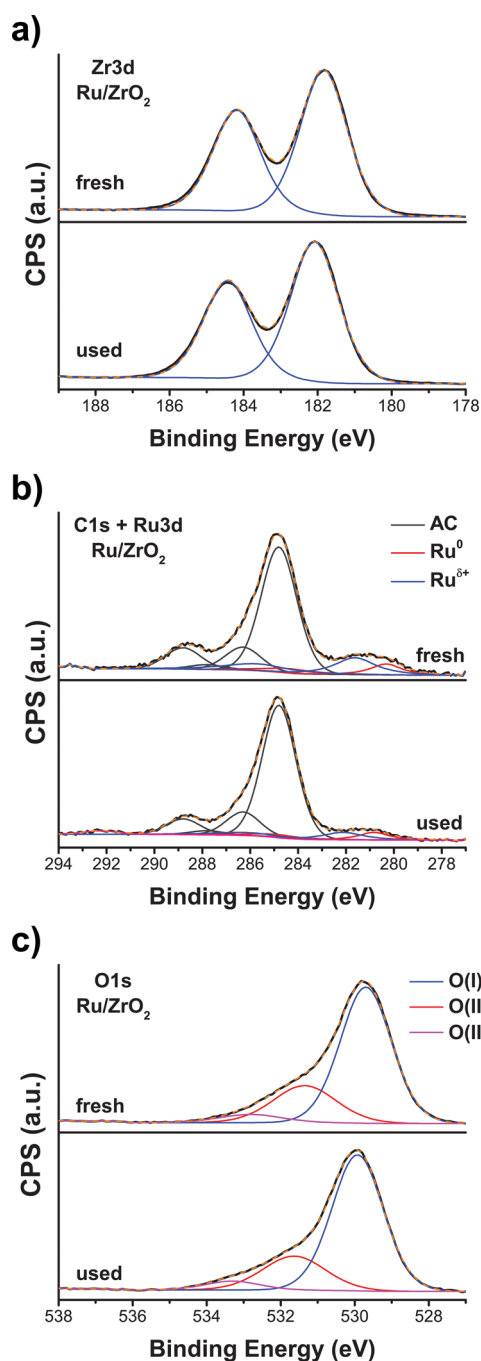
Figure 6. (a) Zr 3d XP spectra, (b) C1S/Ru 3d XP spectra (AC refers adventitious carbon), and (c) O 1s XP spectra of the fresh and five-times recycled Ru/ZrO$_2$ catalysts.

Others have since reported on various alternative methods for titania reduction.[41,50,51] The black coloration of TiO$_2$ is considered to be due to the generation of surface disorder and oxygen vacancies upon H$_2$ reduction.[41] Ru/TiO$_2$ is subjected to much milder conditions in our case (P_{H_2} = 30 bar, T = 423 K; t = 3 h), but it is well-known that transition-metal-promoted titania is more easily reduced by hydrogen spillover effects, which allow the H atoms formed by dissociation on the metal surface to migrate to the reducible oxide.[52]

4.2. FT-IR after CO Adsorption. While the origin of the darkening of the TiO$_2$ is thus established, it is less clear how

this is associated with the actual partial deactivation of the catalyst. The changes in support and their influence on hydrogenation ability were further investigated with low-temperature FT-IR after CO adsorption (CO/FT-IR)[52] on a fresh Ru/TiO$_2$ sample and the catalyst recycled three times. For comparison, two additional samples were characterized: (i) the fresh bare TiO$_2$ (P25) support treated by the same calcination and reduction procedures adopted for the synthesis of the fresh Ru/TiO$_2$ catalyst as well as (ii) the reduced and calcined TiO$_2$ (P25) sample subsequently subjected to the standard conditions of the LA hydrogenation process (e.g., 10 wt % of LA, in dioxane solvent). The fresh titania-only sample had a bluish white color after calcination/reduction, indicating that Ti^{3+} formation already occurs during pretreatment.[53] While temperature-programmed reduction of bare TiO$_2$ (P25) was reported to show reduction of Ti^{4+} species at temperatures higher than 773 K,[45] the color change of the fresh titania-only sample indicates that reduction can also occur under the present pretreatment conditions: i.e., at a temperature that is at least 100 K lower. The color of the titania-only sample subjected to reaction conditions is yellowish because of the deposition of reaction side products, and therefore its color cannot unfortunately be used as an indicator of the oxidation state of the titania. Figure 7 shows the CO stretching region of
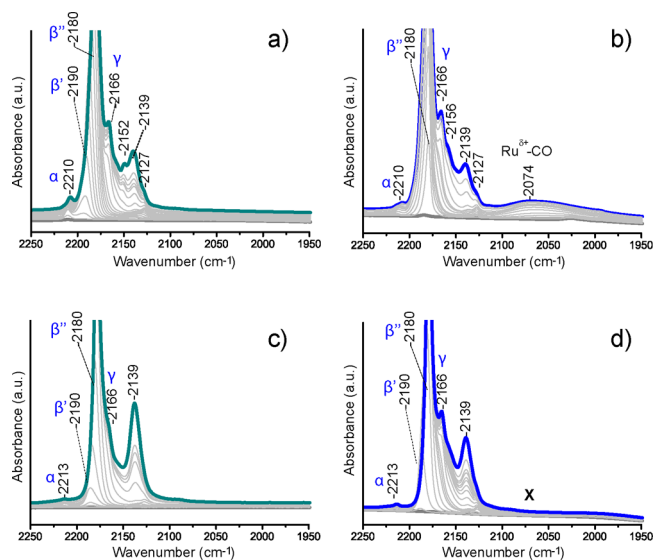

Figure 7. FT-IR spectra upon CO adsorption at 85 K on (a) fresh TiO$_2$, (b) fresh Ru/TiO$_2$, (c) spent TiO$_2$, and (d) three-times-recycled Ru/TiO$_2$ (CO stretching region). Note that the Ru$^{\delta+}$-CO band is not seen in (d).

the FT-IR spectra for the fresh and spent Ru/TiO$_2$ catalysts as well as for the support-only samples upon CO adsorption at 85 K before and after the catalytic treatment. The spectra for fresh TiO$_2$ (P25) correspond well to the results reported by Hadjiivanov et al.,[54,55] with CO adsorption being observed on electrophilic four-coordinated Ti^{4+} α sites (2210 cm^{-1}) and five-coordinated Ti^{4+} β' and β'' sites (2180−2190 cm^{-1});[56] γ sites, five-coordinated Ti^{4+} cations of very low acidity, are observed as well at 2166 cm^{-1}.[54,55] The signals at 2139 and 2152 cm^{-1} belong to physisorbed CO and to CO on surface OH groups, respectively. The latter signal is quite small, given the high degree of surface dehydroxylation after outgassing at 873 K.[57] It should be noted that reduced Ti^{3+} cannot be detected by CO adsorption with FTIR, as CO dissociation

occurs on such sites even at low temperature.[58,59] The CO/FT-IR spectra of fresh Ru/TiO$_2$ (Figure 7b) and fresh TiO$_2$ (Figure 7a) are very similar. A new broad band centered at 2074 cm^{-1} is seen for the fresh Ru/TiO$_2$ catalyst, corresponding to Ru$^{\delta+}$ monocarbonyl species.[60] The spectra of the spent Ru/TiO$_2$ and spent TiO$_2$ samples (Figure 7c,d) also look rather similar, with only a difference in the relative amount of γ sites being noted.

Comparison of the spectra of fresh (Figure 7b) and recycled Ru/TiO$_2$ samples reveals one key difference: the Ru$^{\delta+}$-CO band is absent in the latter. In fact, no Ru carbonyl bands are detected at all. The absence of any such Ru-CO absorption bands on the recycled Ru/TiO$_2$ catalyst can now be related to the decrease in catalytic activity (Figure 2). This lack of CO-accessible Ru sites could be the consequence of encapsulation of the active Ru particles either by collapse of the TiO$_2$ structure or as a result of a strong metal–support interaction effect (SMSI). That the former does not occur for the bulk of the support is evidenced by the XRD patterns of both the fresh and three-times recycled Ru/TiO$_2$ catalysts, which are identical, giving an anatase:rutile ratio of 80:20 for both samples (fresh and spent catalysts).

It should be noted that Di et al. recently also observed a similar reduction of Ti^{4+} to Ti^{3+} in a Ru/TiO$_2$ catalyst used for gas-phase CO oxidation. Prereduction of the catalyst with H$_2$ led to surface reconstruction of the Ru species, as evidenced by HRTEM, with monometallic Ru thought to be responsible for preferential oxidation in their case, as could be seen from CO/FT-IR.[43] Indeed, SMSI effects are known to change the adsorption properties of titania-supported metals exposed to reducing reaction conditions. This phenomenon was first defined by Tauster et al.[61] in 1978 and has since been extensively studied.[58,59,62] Typical of SMSI is the "decoration" or (partial) encapsulation of metal active sites by the migration of support-derived species (e.g., highly mobile TiO$_{2-x}$ suboxide species formed under reducing conditions) onto the metal particles' surface. The SMSI may then either prove advantageous for or detrimental to catalyst activity. For instance, strong metal–support interactions have prevented Ru metal particles from sintering,[63] leading to highly dispersed nanoparticles on the catalyst surface and (usually) to higher activity. Moreover, it has been suggested that partial encapsulation of the active metal by the support might protect the catalyst from deactivation in some cases.[64] On the other hand, a SMSI may negatively affect the performance of the active nanoparticles. For instance, Bonanni et al. attributed the partial loss of catalytic activity in the CO oxidation reaction catalyzed by Pt/TiO$_2$, to encapsulation of the metal clusters by a reduced TiO$_2$ layer.[65]

4.3. STEM. The characterization data detailed above suggest that titania species are reduced under the reaction conditions, become mobile, and gradually encapsulate the Ru nanoparticles, leading to loss of activity. Indeed, the XPS results clearly show the extent to which Ti^{3+} species are formed and additionally show the total Ru to Ti molar ratio to change from 8% for the fresh catalyst to 4% for the Ru/TiO$_2$ catalyst recycled three times. Ru leaching, which could cause the same variation in total Ru/Ti molar ratio, is excluded, as it was previously shown that even under harsher experimental conditions only a negligible amount of Ru (<0.5%) could lixiviate into the solution with this catalyst.[9] Given the lack of sintering, the change in ratio suggests an increase in the amount of TiO$_2$ at the surface: i.e., by coverage of the Ru nanoparticles.

That the loss of active Ru surface is the result of encapsulation of the metal nanoparticles by the support through an SMSI effect was confirmed by STEM measurements on the fresh and three-times recycled Ru/TiO$_2$. The HAADF-STEM images of the fresh Ru/TiO$_2$ material (Figure 8a) show
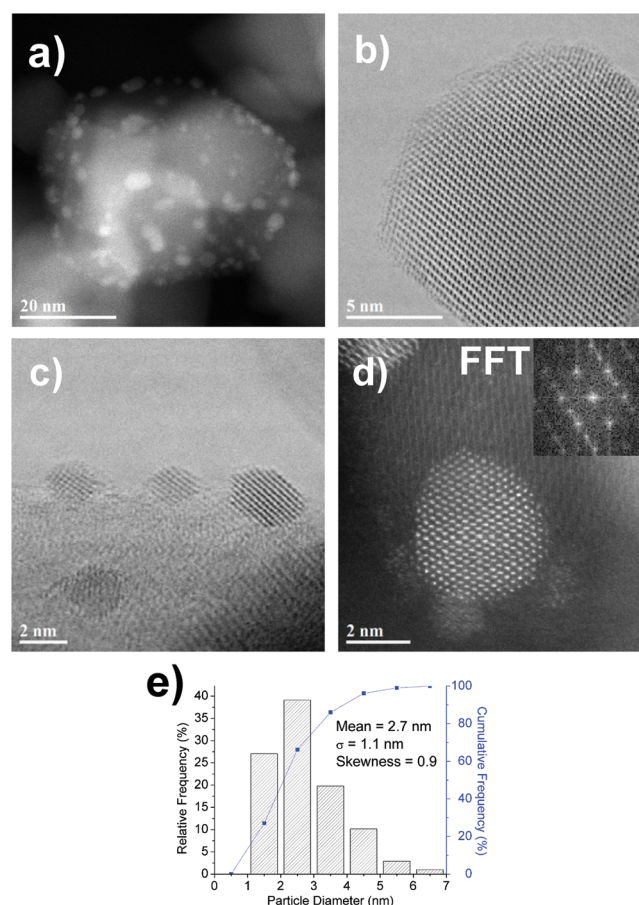

Figure 8. STEM analysis of the fresh Ru/TiO$_2$ catalyst: (a) low-magnification HAADF-STEM image showing typical Ru particle size distribution; (b) BF-STEM image of a typical TiO$_2$ support grain showing "clean" surface facets; (c) BF-STEM image showing a profile view of faceted Ru nanoparticles on the TiO$_2$; (d) atomic resolution HAADF-STEM image and corresponding fast Fourier transform (FFT) (inset) of an individual metallic hcp Ru particle viewed along [100]; (e) measured Ru particle size distribution as extracted from images such as that shown in Figure 8a.

clear evidence of discrete Ru-containing nanoparticles having a mean size of 2.7 nm (Figure 8e). Atomic resolution images of the TiO$_2$ support show it to expose distinct surface facet planes that are very clean (Figure 8b,c). Atomic resolution images of the supported Ru particles confirmed them to be metallic Ru with a hexagonally closed packed (hcp) structure typically exposing {101} and {002} type surface facets (Figure 8c,d).

The STEM analysis of the Ru/TiO$_2$ material recycled three times revealed some definite microstructural changes that correlate well with the drop in catalytic activity, the drop in BET, the observed support reduction, and the loss of active Ru surface area. A population of hcp Ru nanoparticles is still apparent (Figure 9a) with a similar mean particle size of 2.1 nm (Figure 9e). However, on closer inspection, the TiO$_2$ support has clearly developed a continuous disordered surface layer that varies in thickness between 1 and 3 nm (Figure 9b). This
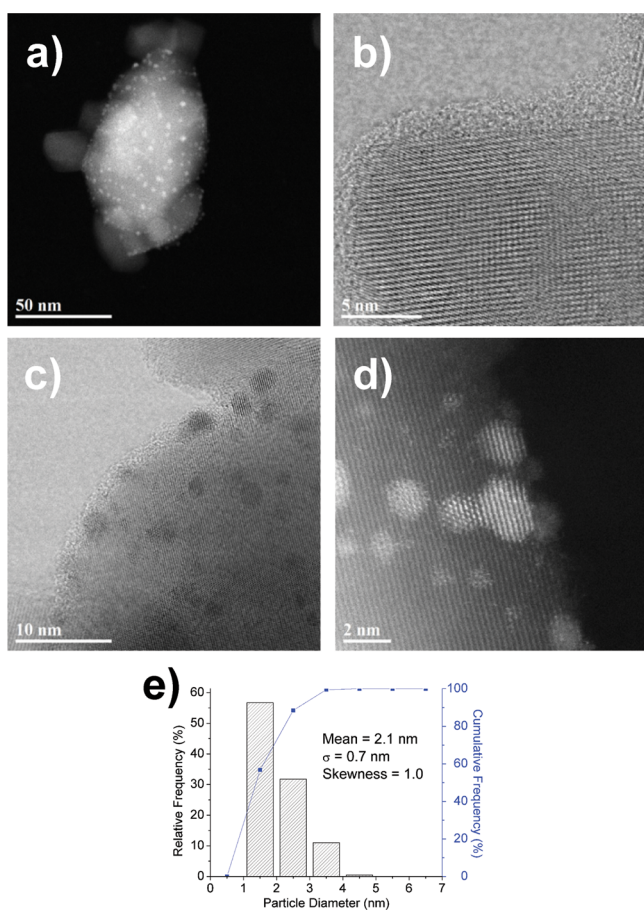
Figure 9. STEM analysis of the Ru/TiO$_2$ catalyst recycled three times: (a) low-magnification HAADF-STEM image showing typical Ru particle size distribution; (b) BF-STEM image of a typical TiO$_2$ support grain showing facets covered with a 1−2 nm thick disordered film; (c) BF-STEM image showing a profile view of Ru nanoparticles embedded in the amorphous over layer covering the TiO$_2$ support; (d) atomic resolution HAADF-STEM image showing individual faceted metallic hcp Ru particles and sub-nanometer clusters; (e) Ru particle size distribution as extracted from images, such as that shown in Figure 9a.
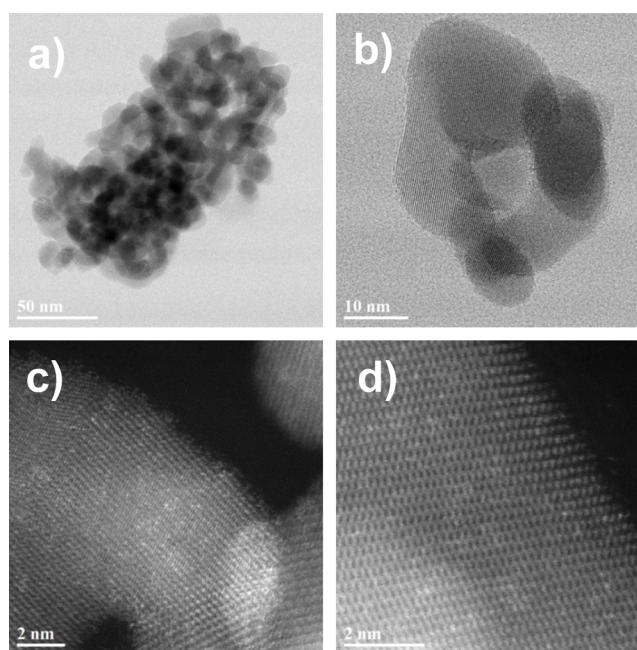
Figure 10. STEM analysis of the fresh Ru/ZrO$_2$ catalyst: representative (a) low- and (b) high-magnification BF-STEM images demonstrating that the ZrO$_2$ agglomerates are devoid of discrete Ru nanoparticles; (c, d) HAADF-STEM images showing atomically dispersed Ru decorating the ZrO$_2$ surface.

amorphization of the titania surface is in line with what has been reported for the 'black hydrogenated titania' synthesis methods.[41,49−51] When viewed in profile, it is apparent that many of the Ru nanoparticles are effectively buried in this thin disordered layer (Figure 9c), which could explain the absence of the Ru$^{\delta+}$-CO band in CO/FT-IR (Figure 7d). It is also interesting to note that a population of sub-nanometer Ru clusters were visible in both the fresh (Figure 8d) and spent (Figure 9d) Ru/TiO$_2$ materials in the HAADF imaging mode.

The STEM images of the fresh, once recycled, and five-times recycled Ru/ZrO$_2$ catalysts show that the microstructural features of the ZrO$_2$ support do not change. This is in line with the lack of change seen by N$_2$ physisorption and by XPS. Surprisingly, the fresh Ru/ZrO$_2$ sample showed no evidence of any Ru-containing nanoparticles on examination by bright field (BF) microscopy (Figure 10a,b). However, in the HAADF-STEM imaging mode (Figure 10c,d) Ru atoms dispersed on the ZrO$_2$ support material could be visualized by virtue of the higher atomic number of Ru ($Z = 44$) in comparison to the atoms making up the support ($Z_{Zr} = 40$, $Z_O = 8$). The Ru atoms were consistently found to be located on Zr column sites. This

is in line with other observations on the location of single atoms on an oxide support.[66] Mostly atomically dispersed Ru atoms have been seen for Ru/Al$_2$O$_3$ together with small Ru aggregates, albeit at a 10 times lower weight loading of Ru.[67] Previously, it was shown that the dispersion of Ru on an oxide support was found to be independent of the metal salt precursor but did depend on the nature of the oxidic support.[68] This would suggest that ZrO$_2$ is responsible for the very high, improved Ru dispersion in our case.

After being recycled for one cycle, the Ru phase of the Ru/ZrO$_2$ material showed some evidence of microstructural evolution, in that the occasional discrete Ru nanoparticle is now detected (Figure 11a,b), although most of the Ru remained in atomically dispersed form. The lattice fringes in some of the particles could be indexed to hcp Ru metal, while others looked to be more disordered in character. A particle size distribution of this rather sparse population of Ru particles showed them to have a mean size of 3.3 nm (Figure 11c). After the fifth reuse, Ru/ZrO$_2$ exhibited many more discrete Ru nanoparticles (Figure 11e), yet a small fraction of atomically dispersed Ru could still be detected on some ZrO$_2$ support grains (Figure 11d). Most of the supported Ru nanoparticles in this sample showed lattice fringe spacings and intersection angles that were consistent with hcp Ru metal. The mean size of this considerably greater population of Ru nanoparticles was measured as 2.8 nm (Figure 11f). The STEM images thus not only confirm that the ZrO$_2$ is stable under the reducing conditions but also reveal some evolution in Ru speciation.

The fact that ZrO$_2$ is not reduced is in line with the work of Eder et al., in which it was shown that higher temperatures (e.g., above 973 K) are needed for ZrO$_2$ reduction.[69] This temperature is significantly higher than the reduction temperature needed to reduce TiO$_2$. The lack of any color change shown by the (bare) ZrO$_2$ support upon calcination, reduction,
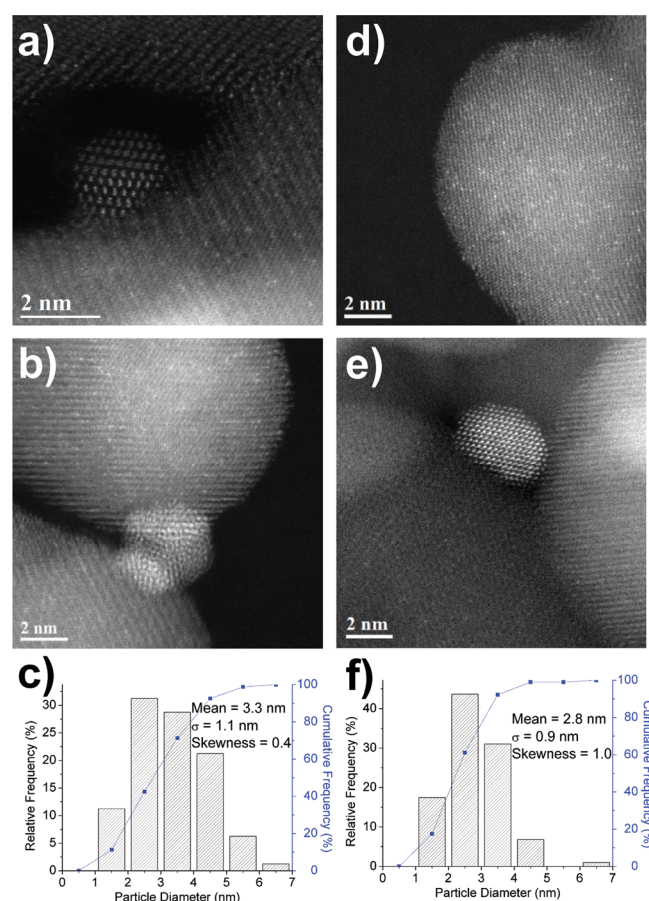
Figure 11. (a, b) STEM analysis of the once-recycled Ru/ZrO$_2$ catalyst: (a) a discrete hcp metallic Ru nanoparticle; (b) example of a more disordered Ru-containing nanoparticle. (c) Measured particle size distribution of the Ru nanoparticles in the once-recycled catalyst (note that monatomic Ru has not been included in this count). (d, e) STEM analysis of the Ru/ZrO$_2$ catalyst recycled five times: (d) atomically dispersed Ru on ZrO$_2$ support; (e) representative example of a metallic hcp Ru nanoparticle. (f) Measured particle size distribution of the Ru nanoparticles in the catalyst recycled five times (note that monatomic Ru has not been included in this count).

and submission to hydrogenation conditions is in line with this. Interestingly, Ruppert et al. also demonstrated that adding ZrO$_2$ to a Pt/TiO$_2$ catalytic system improved its stability by preventing the encapsulation of the metal clusters by TiO$_x$ layers.[70] Further study is now required on how the high dispersion of Ru depends on catalyst preparation parameters, including weight loading and metal precursor, and how the (change in) dispersion affects catalytic activity. Indeed, highly active single-atom catalysts for hydrogenation have been reported.[71] A study on the dependence of specific activity as a function of Ru loading or particle size will provide those insights.

5. CONCLUSIONS

A comparison of the stability of different supported Ru-based catalysts under typical LA hydrogenation conditions in dioxane showed Ru/ZrO$_2$ to perform better than Ru/C and Ru/TiO$_2$, with the former catalyst materials displaying high activity, selectivity, and stability upon repetitive recycling. The Ru/TiO$_2$ catalyst, considered a benchmark catalyst for this reaction, showed clear deactivation upon recycling. This deactivation first became apparent visually by the change in color of this catalyst from gray to dark black. Extensive characterization showed that the deactivation of the Ru/TiO$_2$ catalyst is mainly due to instability of the support and not to sintering of the Ru nanoparticles or fouling. Reduction of the TiO$_2$ support and encapsulation of the Ru nanoparticles as a result of SMSI is thought to be the main cause of catalyst deactivation, as clearly shown by the combination of STEM and XPS data. In Ru/ZrO$_2$, the support did not show any microstructural changes, though some genesis of Ru nanoparticles at the expense of atomically dispersed Ru atoms was observed. The Ru/ZrO$_2$ catalyst displayed stable GVL yields not only in dioxane but also in GVL and other lactones (i.e., γ-hexalactone and γ-octalactone) as more benign solvents. Finally, water was shown to be advantageous for LA hydrogenation.

■ AUTHOR INFORMATION

Corresponding Authors
*E-mail for P.C.A.B.: p.c.a.bruijnincx@uu.nl.
*E-mail for B.M.W.: b.m.weckhuysen@uu.nl.

Notes
The authors declare the following competing financial interest(s): J.F., P.C.A.B., and B.M.W. declare competing financial interests as the work described in this publication is part of a patent application (PCT/EP2016/054031).

■ REFERENCES

(1) Wright, W. R. H.; Palkovits, R. *ChemSusChem* **2012**, *5*, 1657−1667.
(2) Alonso, D. M.; Wettstein, S. G.; Dumesic, J. A. *Green Chem.* **2013**, *15*, 584−595.
(3) Deng, L.; Zhao, Y.; Li, J.; Fu, Y.; Liao, B.; Guo, Q.-X. *ChemSusChem* **2010**, *3*, 1172−1175.
(4) Du, X.-L.; He, L.; Zhao, S.; Liu, Y.-M.; Cao, Y.; He, H.-Y.; Fan, K. *Angew. Chem., Int. Ed.* **2011**, *50*, 7815−7819.
(5) Son, P. A.; Nishimura, S.; Ebitani, K. *RSC Adv.* **2014**, *4*, 10525−10530.
(6) Tang, X.; Hu, L.; Sun, Y.; Zhao, G.; Hao, W.; Lin, L. *RSC Adv.* **2013**, *3*, 10277−10284.
(7) Amarasekara, A. S.; Hasan, M. A. *Catal. Commun.* **2015**, *60*, 5−7.
(8) Chia, M.; Dumesic, J. A. *Chem. Commun.* **2011**, *47*, 12233−12235.
(9) Luo, W.; Deka, U.; Beale, A. M.; van Eck, E. R. H.; Bruijnincx, P. C. A.; Weckhuysen, B. M. *J. Catal.* **2013**, *301*, 175−186.
(10) Al-Shaal, M. G.; Wright, W. R. H.; Palkovits, R. *Green Chem.* **2012**, *14*, 1260−1263.
(11) Joó, F.; Tóth, Z.; Beck, M. T. *Inorg. Chim. Acta* **1977**, *25*, 61−62.
(12) Yuan, J.; Li, S.-S.; Yu, L.; Liu, Y.-M.; Cao, Y.; He, H.-Y.; Fan, K.-N. *Energy Environ. Sci.* **2013**, *6*, 3308−3313.
(13) Mai, E. F.; Machado, M. A.; Davies, T. E.; Lopez-Sanchez, J. A.; Teixeira da Silva, V. *Green Chem.* **2014**, *16*, 4092−4097.
(14) Yan, K.; Chen, A. *Energy* **2013**, *58*, 357−363.

(15) Yan, K.; Liao, J.; Wu, X.; Xie, X. *RSC Adv.* **2013**, *3*, 3853−3856.

(16) Yan, K.; Lafleur, T.; Wu, G.; Liao, J.; Ceng, C.; Xie, X. *Appl. Catal., A* **2013**, *468*, 52−58.

(17) Manzer, L. E. *Appl. Catal., A* **2004**, *272*, 249−256.

(18) Yan, Z.; Lin, L.; Liu, S. *Energy Fuels* **2009**, *23*, 3853−3858.

(19) Galletti, A. M. R.; Antonetti, C.; De Luise, V.; Martinelli, M. *Green Chem.* **2012**, *14*, 688−694.

(20) Lange, J.-P. *Angew. Chem., Int. Ed.* **2015**, *54*, 13186−13197.

(21) Wettstein, S. G.; Bond, J. Q.; Alonso, D. M.; Pham, H. N.; Datye, A. K.; Dumesic, J. A. *Appl. Catal., B* **2012**, *117-118*, 321−329.

(22) Abdelrahman, O. A.; Heyden, A.; Bond, J. *ACS Catal.* **2014**, *4*, 1171−1181.

(23) Upare, P. P.; Lee, J.-M.; Hwang, D.-W.; Halligudi, S. B.; Hwang, Y.-K.; Chang, J.-S. *J. Ind. Eng. Chem.* **2011**, *17*, 287−292.

(24) Lange, J.-P.; Price, R.; Ayoub, P.; Louis, J.; Petrus, L.; Clarke, L.; Gosselink, H. *Angew. Chem., Int. Ed.* **2010**, *49*, 4479−4483.

(25) Ruppert, A. M.; Grams, J.; Jedrzejczyk, M.; Matras-Michalska, J.; Keller, N.; Ostojska, K.; Sautet, P. *ChemSusChem* **2015**, *8*, 1538−1547.

(26) Abdelrahman, O. A.; Luo, H. Y.; Heyden, A.; Román-Leshkov, Y.; Bond, J. Q. *J. Catal.* **2015**, *329*, 10−21.

(27) Luo, W.; Sankar, M.; Beale, A. M.; He, Q.; Kiely, C. J.; Bruijnincx, P. C. A.; Weckhuysen, B. M. *Nat. Commun.* **2015**, *6*, 6540.

(28) Cao, S.; Monnier, J. R.; Williams, C. T.; Diao, W.; Regalbuto, J. R. *J. Catal.* **2015**, *326*, 69−81.

(29) Yang, Y.; Gao, G.; Zhang, X.; Li, F. *ACS Catal.* **2014**, *4*, 1419−1425.

(30) Braden, D. J.; Henao, C. A.; Heltzel, J.; Maravelias, C. C.; Dumesic, J. A. *Green Chem.* **2011**, *13*, 1755−1765.

(31) Yao, Y.; Wang, Z.; Zhao, S.; Wang, D.; Wu, Z.; Zhang, M. *Catal. Today* **2014**, *234*, 245−250.

(32) Ftouni, J.; Villandier, N.; Auneau, F.; Besson, M.; Djakovitch, L.; Pinel, C. *Catal. Today* **2015**, *257*, 267−273.

(33) Guo, X.; Guan, J.; Li, B.; Wang, X.; Mu, X.; Liu, H. *Sci. Rep.* **2015**, *5*, 16451.

(34) Craig, J. B. *Talanta* **1991**, *38*, 812−817.

(35) Prat, D.; Hayler, J.; Wells, A. *Green Chem.* **2014**, *16*, 4546−4551.

(36) Wang, D.; Hakim, S. H.; Martin Alonso, D.; Dumesic, J. A. *Chem. Commun.* **2013**, *49*, 7040−7042.

(37) Aoshima, A.; Tonomura, S.; Fukui, H.; Imai, H. Process Prod. polyether polyol and a product. U.S. Patent 4,658,065, 1987.

(38) Tan, J.; Cui, J.; Deng, T.; Cui, X.; Ding, G.; Zhu, Y.; Li, Y. *ChemCatChem* **2015**, *7*, 508−512.

(39) Michel, C.; Zaffran, J.; Ruppert, A. M.; Matras-Michalska, J.; Jedrzejczyk, M.; Grams, J.; Sautet, P. *Chem. Commun.* **2014**, *50*, 12450−12453.

(40) Naumkin, A.; Kraut-Vass, A.; Gaarenstroom, S. W.; Powell, C. J. *NIST X-ray Photoelectron Spectroscopy Database*; www.srdata.nist.gov/xps/, accessed February 2015.

(41) Lin, T.; Yang, C.; Wang, Z.; Yin, H.; Lu, X.; Huang, F.; Lin, J.; Xie, X.; Jiang, M. *Energy Environ. Sci.* **2014**, *7*, 967−972.

(42) Biesinger, M. C.; Lau, L. W. M.; Gerson, A. R.; Smart, R. S. C. *Appl. Surf. Sci.* **2010**, *257*, 887−898.

(43) Di, L.; Wu, G.; Dai, W.; Guan, N.; Li, L. *Fuel* **2015**, *143*, 318−326.

(44) Omotoso, T.; Boonyasuwat, S.; Crossley, S. P. *Green Chem.* **2014**, *16*, 645−652.

(45) Pham, T. N.; Sooknoi, T.; Crossley, S. P.; Resasco, D. E. *ACS Catal.* **2013**, *3*, 2456−2473.

(46) Barr, T. L.; Seal, S. *J. Vac. Sci. Technol., A* **1995**, *13*, 1239−1246.

(47) Sayan, Ş.; Süzer, Ş.; Uner, D. O. *J. Mol. Struct.* **1997**, *410−411*, 111−114.

(48) Barreca, D.; Battiston, G. A.; Gerbasi, R.; Tondello, E.; Zanella, P. *Surf. Sci. Spectra* **2000**, *7*, 303−309.

(49) Chen, X.; Liu, L.; Yu, P. Y.; Mao, S. S. *Science* **2011**, *331*, 746−750.

(50) Yang, C.; Wang, Z.; Lin, T.; Yin, H.; Lü, X.; Wan, D.; Xu, T.; Zheng, C.; Lin, J.; Huang, F.; Xie, X.; Jiang, M. *J. Am. Chem. Soc.* **2013**, *135*, 17831−17838.

(51) Wang, Z.; Yang, C.; Lin, T.; Yin, H.; Chen, P.; Wan, D.; Xu, F.; Huang, F.; Lin, J.; Xie, X.; Jiang, M. *Adv. Funct. Mater.* **2013**, *23*, 5444−5450.

(52) Pham, T. N.; Shi, D.; Sooknoi, T.; Resasco, D. E. *J. Catal.* **2012**, *295*, 169−178.

(53) Hadjiivanov, K.; Lavalley, J.-C.; Lamotte, J.; Maugé, F.; Saint-Just, J.; Che, M. *J. Catal.* **1998**, *176*, 415−425.

(54) Hadjiivanov, K.; Lamotte, J.; Lavalley, J.-C. *Langmuir* **1997**, *13*, 3374−3381.

(55) Hadjiivanov, K. I.; Klissurski, D. G. *Chem. Soc. Rev.* **1996**, *25*, 61−69.

(56) Minella, M.; Faga, M. G.; Maurino, V.; Minero, C.; Pelizzetti, E.; Coluccia, S.; Martra, G. *Langmuir* **2010**, *26*, 2521−2527.

(57) Martra, G. *Appl. Catal., A* **2000**, *200*, 275−285.

(58) Haller, G. L.; Resasco, D. E. *Adv. Catal.* **1989**, *36*, 173−253.

(59) Vannice, M. A. *Catal. Today* **1992**, *12*, 255−267.

(60) Abhivantanaporn, P. *J. Catal.* **1972**, *27*, 56−59.

(61) Tauster, S. J.; Fung, S. C.; Garten, R. L. *J. Am. Chem. Soc.* **1978**, *100*, 170−175.

(62) Pesty, F.; Steinrück, H.-P.; Madey, T. E. *Surf. Sci.* **1995**, *339*, 83−95.

(63) Hou, Z.; Yashima, T. *Appl. Catal., A* **2004**, *261*, 205−209.

(64) Chenakin, S. P.; Melaet, G.; Szukiewicz, R.; Kruse, N. *J. Catal.* **2014**, *312*, 1−11.

(65) Bonanni, S.; Aït-Mansour, K.; Brune, H.; Harbich, W. *ACS Catal.* **2011**, *1*, 385−389.

(66) Liang, S.; Hao, C.; Shi, Y. *ChemCatChem* **2015**, *7*, 2559−2567.

(67) Kwak, J. H.; Kovarik, L.; Szanyi, J. *ACS Catal.* **2013**, *3*, 2449−2455.

(68) Vasiliadou, E. S.; Heracleous, E.; Vasalos, I. A.; Lemonidou, A. A. *Appl. Catal., B* **2009**, *92*, 90−99.

(69) Eder, D.; Kramer, R. *Phys. Chem. Chem. Phys.* **2002**, *4*, 795−801.

(70) Ruppert, A. M.; Paryjczak, T. *Appl. Catal., A* **2007**, *320*, 80−90.

(71) Yang, X.-F.; Wang, A.; Qiao, B.; Li, J.; Liu, J.; Zhang, T. *Acc. Chem. Res.* **2013**, *46*, 1740−1748.